



# Sol–Gel Synthesis of Dy-Substituted $\text{Ni}_{0.4}\text{Cu}_{0.2}\text{Zn}_{0.4}(\text{Fe}_{2-x}\text{Dy}_x)\text{O}_4$ Nano Spinel Ferrites and Evaluation of Their Antibacterial, Antifungal, Antibiofilm and Anticancer Potentialities for Biomedical Application

Mohammad Azam Ansari<sup>1</sup>   
 Sultan Akhtar<sup>2</sup>   
 Mohd Ahmar Rauf<sup>3</sup>  
 Mohammad N Alomary<sup>4</sup>   
 Sami AlYahya<sup>4</sup>  
 Saad Alghamdi<sup>5</sup>   
 MA Almessiere<sup>2,6</sup>  
 Abdulhadi Baykal<sup>7</sup>  
 Firdos Khan<sup>8</sup>   
 Syed Farooq Adil<sup>9</sup>   
 Mujeeb Khan<sup>9</sup>   
 Mohammad Rafe Hatshan<sup>9</sup> 

<sup>1</sup>Department of Epidemic Disease Research, Institute for Research & Medical Consultations (IRMC), Imam Abdulrahman Bin Faisal University, Dammam, 31441, Saudi Arabia; <sup>2</sup>Department of Biophysics, Institute for Research & Medical Consultation (IRMC), Imam Abdulrahman Bin Faisal University, Dammam, 31441, Saudi Arabia; <sup>3</sup>Department of Surgery, Miller School of Medicine, University of Miami, Miami, FL, USA; <sup>4</sup>National Centre for Biotechnology, King Abdulaziz City for Science and Technology (KACST), Riyadh, 11442, Saudi Arabia; <sup>5</sup>Laboratory Medicine Department, Faculty of Applied Medical Sciences, Umm Al-Qura University, Makkah, Saudi Arabia; <sup>6</sup>Department of Physics, College of Science, Imam Abdulrahman Bin Faisal University, Dammam, 31441, Saudi Arabia; <sup>7</sup>Department of Nanomedicine Research, Institute for Research & Medical Consultations (IRMC), Imam Abdulrahman Bin Faisal University, Dammam, 31441, Saudi Arabia; <sup>8</sup>Department of Stem Cell Research, Institute for Research and Medical Consultations (IRMC), Imam Abdulrahman Bin Faisal University, Dammam, 31441, Saudi Arabia; <sup>9</sup>Department of Chemistry, College of Science, King Saud University, Riyadh, 11451, Kingdom of Saudi Arabia

Correspondence: Mohammad Azam Ansari; Syed Farooq Adil  
 Email maansari@iau.edu.sa; sfadil@ksu.edu.sa

**Background:** The constant rise of microbial biofilm formation and drug resistance to existing antimicrobial drugs poses a significant threat to community health around the world because it reduces the efficacy and efficiency of treatments, increasing morbidity, mortality, and health-care expenditures. As a result, there is an urgent need to develop novel antimicrobial agents that inhibit microbial biofilm formation.

**Methods:** The  $[\text{Ni}_{0.4}\text{Cu}_{0.2}\text{Zn}_{0.4}](\text{Fe}_{2-x}\text{Dy}_x)\text{O}_4$  ( $x \leq 0.04$ ) (Ni-Cu-Zn) nano spinel ferrites (NSFs) have been synthesized by the sol–gel auto-combustion process and were characterized by X-ray diffraction (XRD), scanning electron microscopy (SEM), energy dispersive x-ray (EDX) and transmission electron microscopy (TEM). The antimicrobial, antibiofilm and antiproliferative activities of Ni-Cu-Zn NSFs were also examined.

**Results:** The XRD pattern confirms the secondary phase  $\text{DyFeO}_3$  and  $\text{Fe}_2\text{O}_3$  for substituted  $\text{Dy}^{3+}$  samples, and the crystallite size ranged from 10 to 19 nm. TEM analysis of NSFs revealed that the particles were cube-shaped and 15nm in size. NSFs exhibited significant antimicrobial, antibiofilm and antiproliferative activity. At concentration of 1 mg/mL, it was found that the NSFs (ie,  $x=0.0$ ,  $x=0.01$ ,  $x=0.02$ ,  $x=0.03$  and  $x=0.04$ ) inhibit biofilm formation by 27.6, 26.2, 58.5, 33.3 and 25% for methicillin-resistant *Staphylococcus aureus* (MRSA) and 47.5, 43.5, 48.6, 58.3 and 26.6% for *Candida albicans*, respectively. SEM images demonstrate that treating MRSA and *C. albicans* biofilms with NSFs significantly reduces cell adhesion, colonization and destruction of biofilm architecture and extracellular polymeric substances matrices. Additionally, SEM and TEM examination revealed that NSFs extensively damaged the cell walls and membranes of MRSA and *C. albicans*. Huge ultrastructural alteration such as deformation, disintegration and separation of cell wall and membrane from the cells was observed, indicating significant loss of membrane integrity, which eventually led to cell death. Furthermore, it was observed that NSF inhibited the cancer cell growth and proliferation of HCT-116 in a dose-dependent manner.

**Conclusion:** The current study demonstrated that the synthesized Ni-Cu-Zn NSFs could be used to develop potential antimicrobial surface coatings agents for a varieties of biomedical-related materials and devices in order to prevent the biofilms formation and their colonization. Furthermore, the enhanced antiproliferative properties of manufactured SNFs suggest a wide range of biomedical applications.

**Keywords:** biomedical application, nano spinel ferrites, MRSA, *Candida albicans*, biofilm, ultrastructural alteration

## Introduction

The study and application of nanomaterials has grown in recent years because a nano-sized object exhibits different properties of its bulk materials due to changes in its surface-volume ratio. In many biochemical reactions and a number of applications in different industries, most nanomaterials have shown excellent quantum confinement with unique catalysis properties to improve the technique for electronic, environmental, and biomedical purposes.<sup>1,2</sup> The primary application areas for new spinel ferrite include diverse manufacturing applications such as data storage, radar absorption, telecommunications, negligible eddy current loss, microwaves, permanent magnets, sensors, ferrofluids, hydrogen processing, alcoholic decomposition, oxidizing dehydrogenation, electrocatalytic operation, and corrosion resistance.<sup>3-5</sup>

A significant trend in Ni-Cu spinel behaviour has recently been demonstrated in soft ferromagnetic ceramic materials, which have found widespread use in various applications, including touch, home appliances, computers, inductors, transformers, recording heads, hyperthermia systems, cancer cell therapy, magnetic resonance imaging (MRI), multilayer chip inductor (MLCI) and more applications.<sup>6-8</sup> Recently, the potential biomedical applications of spinel ferrites nanomaterials have gained much attention, due to their cost-effectiveness, easy availability, extraordinary stability, and biocompatibility.<sup>9-14</sup> The advantages of metal and metal oxide nanoparticles in biomedical applications have already been reported against a wide range of life-threatening drug-resistant bacteria and cancerous cells.<sup>3,10,11,15</sup> Naskar et al<sup>16</sup> recently showed that an Ag-ZnO nanocomposite conjugated with erythromycin antibiotics has excellent antibacterial activity against MRSA clinical isolates, as well as good biocompatibility and high cell viability in HEK293 cells. Another study found that when MDR *S. aureus* is exposed to near-infrared light, Au-ZnO coupled with black phosphorus suppresses its growth.<sup>17</sup> Cho et al<sup>18</sup> reported the antibacterial activity of nickel doped zinc oxide conjugated black phosphorus nanocomposite and its synergistic activity with polymyxin B against polymyxin-resistant *E. coli* carrying colistin resistance gene *mcr-1* and found that the nanocomposite was biocompatible with HEK293 cells and polymyxin B. Several studies have been conducted in-depth to explore the unusual characteristics of Ni-Cu ferrites and it was concluded that these characteristics are due to favoured distributions of Fe<sup>3+</sup> and Fe<sup>2+</sup> cations into the tetrahedral and octahedral sub-lattice sites in the crystal structure.<sup>19,20</sup> Spinel ferrite nanoparticles can be synthesized using various

techniques, including co-precipitation, citrate-assisted auto-combustion, hydrothermal, reverse micelle, microwave synthesis, sol-gel and ultrasonication. A considerable number of scientific studies have been performed on metal substituted spinel ferrite nanoparticles. Nickel-copper-zinc ferrites, synthesized through the various methods, has MLCI applications.<sup>7,21</sup> Copper and cobalt ferrite nanoparticles have been shown to have antibacterial and antifungal action against Gram-negative *E. coli*, Gram-positive *S. aureus*, and *C. albicans* in some experiments.<sup>9-11</sup> There is a scarcity of literature on the antibacterial and anticandidal activity of metal-substituted NSF's and, most importantly, no study has been reported on antibiofilm potential and electron microscopic ultrastructural alteration caused by metal-substituted NSF's in bacteria and *Candida*. In this perception, the objective of present work was (i) synthesis of [Ni<sub>0.4</sub>Cu<sub>0.2</sub>Zn<sub>0.4</sub>](Fe<sub>2-x</sub>Dy<sub>x</sub>)O<sub>4</sub> (x ≤ 0.04) NSF's by sol-gel approach, (ii) Characterization of their structural, morphological, and optical properties by XRD, SEM, TEM and EDX, (iii) investigation of antibacterial and anticandidal activity of synthesized NSF's against methicillin-resistant *Staphylococcus aureus* (MRSA) and *Candida albicans*, (iv) investigation of antibiofilm activity of synthesized NSF's against MRSA and *C. albicans*, (v) investigation of effects of NSF on biofilm structure of MRSA and *C. albicans* as examined by SEM, and (vi) investigation of ultrastructural alteration caused by NSF's on MRSA and *C. albicans* by SEM and TEM.

## Materials and Methods

### Synthesis and Characterization of [Ni<sub>0.4</sub>Cu<sub>0.2</sub>Zn<sub>0.4</sub>](Fe<sub>2-x</sub>Dy<sub>x</sub>)O<sub>4</sub> (x ≤ 0.04) Nano Spinel Ferrites (Ni-Cu-Zn NSF's)

The [Ni<sub>0.4</sub>Cu<sub>0.2</sub>Zn<sub>0.4</sub>](Fe<sub>2-x</sub>Dy<sub>x</sub>)O<sub>4</sub> (x ≤ 0.04) NSF's prepared by citrate sol-gel auto-combustion technique. The metal salts; NiCl<sub>2</sub>·6H<sub>2</sub>O (p.a., ≥98%, Sigma Aldrich), Zn(NO<sub>3</sub>)<sub>2</sub>·6H<sub>2</sub>O (p.a., 98%, Sigma Aldrich), Cu(NO<sub>3</sub>)<sub>2</sub>·2.5H<sub>2</sub>O (p.a., 98%, Sigma Aldrich), (Fe(NO<sub>3</sub>)<sub>3</sub>·9H<sub>2</sub>O (p.a., ≥98%, Sigma Aldrich), Dy(NO<sub>3</sub>)<sub>3</sub>·xH<sub>2</sub>O (p.a., 99.9%, Sigma Aldrich), and citric acid (C<sub>6</sub>H<sub>8</sub>O<sub>7</sub>) (p.a., ≥99.5%, Sigma Aldrich) were thawed in distilled water and stirred continually at 95°C for 45 min to form a homogeneous mixture. The pH of the resulting mixture was kept at 7 by adding ammonia solution; then, the hot plate was adjusted at 115°C for 1 hour, then 375°C with constant stirring until the solution became gel and burnt to obtain the Ni-Cu-Zn NSF's powder.

The crystalline of synthesized NSF was identified with X-ray powder pattern Rigaku Benchtop Miniflex (Cu K $\alpha$  radiation at room temperature,  $2\theta = 20^\circ\text{--}70^\circ$ ). The microstructure was portrayed by SEM, TEM and EDX (FEI Titan ST with EDX).

## Antibacterial, Anticandidal and Anti-Biofilm Studies of Ni-Cu-Zn NSF Strains

*C. albicans* and methicillin-resistant *S. aureus* (MRSA) were used to investigate the anticandidal, antibacterial, and antibiofilm activity of Ni-Cu-Zn NSF.

### Antibacterial Activity by Determining Minimum Inhibitory Concentration (MIC) and Minimum Bactericidal Concentration (MBC)

#### MIC

The two-fold serial dilution technique described by Ansari et al<sup>22</sup> was used to determine the MIC and MBC values of NSF against MRSA. In brief,  $1 \times 10^7$  CFU/mL bacterial culture were treated with NSF ( $x=0.0, 0.01, 0.02, 0.03,$  and  $0.04$ ) at concentrations ranging from 1 to 32 mg/mL, and then the treated and untreated samples were incubated for 24 h at  $37^\circ\text{C}$ . The MIC was established as the lowest concentration of antimicrobial drugs that prevented observable bacterial growth.<sup>22</sup>

#### MBC

After MIC assessment, MBC was determined by spreading 100  $\mu\text{L}$  aliquots from culture wells when no apparent growth was detected on MHA plates and the plates were subsequently incubated for 24 h at  $37^\circ\text{C}$ . The lowest concentration of NSF that kills 100% of the population of the tested organism was considered as MBC value.<sup>22</sup>

### Evaluation of the Anti-Candida Activity of NSF by Colony-Forming Unit (CFU)

As-synthesized Ni-Cu-Zn NSF were used for assessment of antifungal activity against *C. albicans*, an opportunistic yeast. The freshly grown culture of yeast cells in SDB was obtained by washing with PBS, and cell density was adjusted to 0.5 McFarland before performing the antifungal test.

Colony-forming units (CFU) were determined by adding 2 mg/mL of synthesized Ni-Cu-Zn NSF to tubes containing 0.5 mL of 0.6 McFarland *Candida* cells. Prior to treatment, the NSF were sonicated for 20 min to obtain a homogeneous nanomaterial solution. The

NSF treated and untreated (control) *C. albicans* were incubated for 28 h at  $28 \pm 2^\circ\text{C}$  at 150 rpm in a rotary shaker incubator. The number of viable cells was determined by counting CFU to assess the antifungal activity of the NSF. After incubation, the treated and untreated sample was serially diluted, and subsequently, 100  $\mu\text{L}$  was plated on SDA plates and further incubated for 28–32 h at  $28 \pm 2^\circ\text{C}$ . After that, colonies were counted, and the formula calculated the percent survival rate (SR%) of *C. albicans*,  $\text{SR}\% = (A/B) \times 100$  (where A= number of CFU of the treated sample; B: number of CFU of untreated control sample).

### Effect of Ni-Cu-Zn NSF on MRSA and *C. albicans* Biofilm

The biofilm inhibition of MRSA and *C. albicans* after treatment with Ni-Cu-Zn NSF was investigated by crystal violet assay.<sup>22</sup> In brief, freshly grown cultures of MRSA and *C. albicans* treated with varying concentrations of Ni-Cu-Zn NSF in 96 microtiter plates were incubated at  $37^\circ\text{C}$  and  $28^\circ\text{C}$  for 24 h, respectively. The MRSA and *C. albicans* without any Ni-Cu-Zn NSF treatments were taken as control. Following the incubation period, all contents were decanted from wells, washed with PBS, and stained with crystal violet (0.1% w/v) for 30 minutes, washed again with PBS, and then air dried. The stained biofilm was solubilized with ethyl alcohol (95%) and optical density was measured at 595 nm.<sup>23</sup> The percentage of biofilm inhibition was estimated using the equation below:

$$\% \text{Biofilm inhibition} = \left\{ \frac{(\text{OD of control} - \text{OD of tested samples})}{(\text{OD of control})} \right\} \times 100$$

### Visualization of Biofilm Architecture by SEM

The effect of Ni-Cu-Zn NSF on MRSA and *C. albicans* biofilm structure was further examined by SEM as described in our previous work.<sup>22</sup> Briefly, 100  $\mu\text{L}$  of MRSA and *C. albicans* cultures were inoculated on glass coverslips in the absence and presence of Ni-Cu-Zn NSF for 24 h at the recommended temperature. The glass coverslips were then removed, washed with PBS, fixed with glutaraldehyde (2.5% v/v), washed with PBS again, dehydrated with a series of ethyl alcohol, and finally air-dried. After that, the samples were coated with gold and then

finally, the images of treated and untreated biofilm structure of MRSA and *C. albicans* were collected by using SEM.<sup>22</sup>

## Mechanism of Interaction of NSF's with Bacterial and Candida Cells

### Visualization of Effects of NSF's on the Morphology of MRSA and *C. albicans*: SEM Study

SEM investigated the topological alteration in MRSA and *C. albicans* after treatment with Ni-Cu-Zn NSF's. MRSA and Candida cells ( $10^6$  CFU/mL) were treated with 0.5 and 1 mg/mL of NSF's for 18 h at 37°C and 28°C, respectively. After incubation, the treated and untreated samples were centrifuged at 12,000 rpm for 10 min, and collected pellets were washed twice with PBS. After washing, all the samples were fixed with primary fixative (2.5% glutaraldehyde) followed by secondary fixative (1% osmium tetroxide). After fixation, dehydration was carried out with 30%, 50%, 70%, 80%, 90%, and 100% of ethyl alcohol. After that, the samples were fixed on the aluminum stubs and left for complete drying, and then the samples were coated with gold and finally, the effects of NSF's on the morphology of MRSA and *C. albicans* were observed under a scanning electron microscope at an accelerating voltage of 20 kV.<sup>24</sup>

### Ultrastructural Alteration in Bacteria and Candida Cells Caused by NSF's: TEM Analysis

The ultrastructural alteration in MRSA and Candida after treatment with Ni-Cu-Zn NSF's was further investigated by TEM. To examine the interaction of NSF's with MRSA and *C. albicans*, the cells were grown in TSB and SDB at 37°C and  $28 \pm 2^\circ\text{C}$  overnight. The freshly grown cultures were pelleted by centrifugation. The MRSA and *C. albicans* cells ( $10^6$  CFU/mL) were then treated with NSF's and then further incubated at a similar condition, as mentioned above, in a shaker incubator at 150 rpm. The MRSA and *C. albicans* without any NSF's treatment were taken as control. After incubation, the treated and untreated samples were washed twice; pellets were collected and fixed with primary fixative (2.5% glutaraldehyde) followed by secondary fixative (1% osmium tetroxide) and dehydration process.<sup>25</sup> After that, the samples were embedded in resin overnight for polymerization. Then, ultra-thin sections were made using a microtome diamond knife, then stained with uranyl acetate followed by counterstained lead citrate (4%) and then mounted on carbon-coated copper grids.

Finally, the ultrastructural alteration caused by NSF's in MRSA and *C. albicans* cells was recorded by TEM, Technai, FEI, USA.<sup>25</sup>

### Cytotoxic Activity

In this study, human colorectal carcinoma (HCT-116) was used to investigate the cytotoxic effects of NSF's on their viability and proliferation. The cells were cultured and maintained in the DMEM media supplemented with L-glutamine (5%), penicillin (1%), streptomycin (1%), FBS (10%), and selenium chloride (1%) and were grown at 37°C under 5% CO<sub>2</sub> atmosphere. The cell viability activity and alteration in DNA of HCT-116 cell line after treatment with NSF's was examined by MTT and DAPI staining assay, respectively, according to previous report.<sup>26</sup> Briefly, the cells were treated with varying concentrations of NSF's ( $X=0.02$  and  $x=0.03$ ) in a 96 well culture plates. As a control group, cells were cultured without NSF's. After 48 h of incubation, 10  $\mu\text{L}$  of MTT (5 mg/mL) solution was added into each well and plates were then further incubated in a CO<sub>2</sub> incubator for 4 h. After that, the MTT solution was replaced with DMSO (1%), and the 96-well plate was then examined under an ELISA plate reader at a wavelength of 570 nm. The data are presented as mean ( $\pm$ ) standard deviation (SD) obtained from triplicates.

Further, the DAPI staining assay was used to examine the changes in the DNA of cancer cells after treatment with NSF's using protocol described by Alahmari et al.<sup>27</sup> Briefly, the HCT-116 cells were divided into two groups, the control group ie, without NSF's and the experimental group ie, treated with 35  $\mu\text{g/mL}$  of NSF's ( $x=0.02$  and  $x=0.03$ ). Post 48 h treatment, both groups were exposed to ice-cold paraformaldehyde (4%) and then with Triton X-100 in PBS. After that, cells were stained with DAPI (1  $\mu\text{g/mL}$ ) for 5 min at 37°C in the dark, and excess dye was removed by washing with PBS. Changes in DNA of HCT-116 cells were examined by using a confocal scanning microscope (Zeiss, Germany).

## Results and Discussion

### Characterization of Ni-Cu-Zn NSF's

The XRD patterns of  $[\text{Ni}_{0.4}\text{Cu}_{0.2}\text{Zn}_{0.4}](\text{Fe}_{2-x}\text{Dy}_x)\text{O}_4$  ( $x \leq 0.4$ ) NSF's are shown in Figure 1. The pure phases of Ni-Cu-Zn spinel ferrites were observed from the XRD patterns peaks for all ratios without any impurity. Besides, the most intense peak (311) stayed in the same position when increasing the Dy content because the cubic shape of the

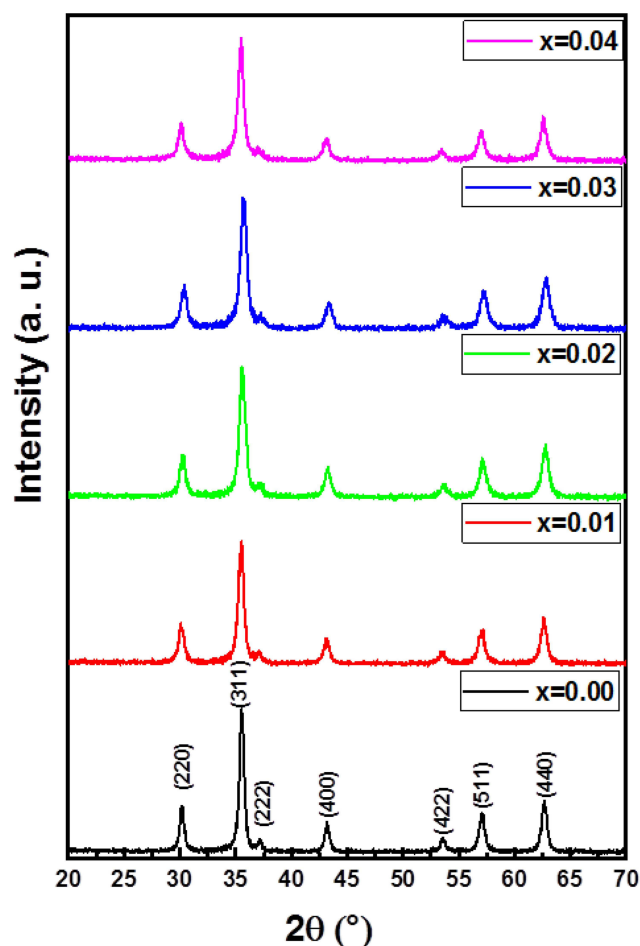


Figure 1 XRD pattern of  $[\text{Ni}_{0.4}\text{Cu}_{0.2}\text{Zn}_{0.4}](\text{Fe}_{2-x}\text{Dy}_x)\text{O}_4$  ( $x \leq 0.4$ ) NSFs.

spinel lattice was retained. The cell constant, an average of crystal size ( $D_{\text{XRD}}$ ) and goodness of refinement resulted from Rietveld refinement with FullProf software are provided in Table 1. The refinement revealed that the cell constant ( $a$ ) was growing with increasing the amount of Dy as attributable to the expansion in spinel crystal. The  $D_{\text{XRD}}$  was determined by Scherer's equation, which shows that the crystallite size was between 10 and 19 nm.

Table 1 Dy Content, Refined Structural Parameters for  $[\text{Ni}_{0.4}\text{Cu}_{0.2}\text{Zn}_{0.4}](\text{Fe}_{2-x}\text{Dy}_x)\text{O}_4$  ( $x \leq 0.4$ ) NSFs

x	a (Å)	V (Å) <sup>3</sup>	$D_{\text{XRD}}$ (nm) ±0.05
0.00	8.392(5)	591.13	17.19
0.01	8.393(4)	591.32	15.51
0.02	8.397(1)	592.09	13.54
0.03	8.402(9)	593.31	12.01
0.04	8.408(2)	594.43	10.77

Figure 2 depicts SEM images of Ni-Cu-Zn NSFs that were roughly conglomerated and spherical in shape. The EDX spectrum confirmed the presence of Ni, Cu, Zn, Fe, Dy and O (Figure 3). TEM images of Ni-Cu-Zn NSFs are shown in the figure showed that the particles were cube-shaped and exhibited aggregation because of their magnetic nature. The size dispersal was found between 15 nm (Figure 4). The particle size estimation results were well-agreed with the crystallite sizes revealed by XRD refinements (Table 1).

## Antibacterial Activity by Determining MIC and MBC

In the present study, the antibacterial activity of  $[\text{Ni}_{0.4}\text{Cu}_{0.2}\text{Zn}_{0.4}](\text{Fe}_{2-x}\text{Dy}_x)\text{O}_4$  ( $x=0, 0.01, 0.02, 0.03$  and  $0.04$ ) NSFs was evaluated against gram-positive MRSA using the microbroth dilution method by determining their MICs and MBCs.<sup>28</sup> The MICs/MBCs values of sample  $x=0, 0.01, 0.02, 0.03$  and  $0.04$  NSFs against MRSA were found in the range of 4/16, 8/24, 2/8, 4/16 and 8/24 mg/mL, respectively (Figure 5). MIC and MBC results showed that sample  $x=0.02$  showed the highest bacteriostatic and bactericidal activities. In a previous study, it has been reported that chromium-substituted spinel copper ferrite  $[(\text{CuCr}_x\text{Fe}_{2-x}\text{O}_4$  ( $0.0 \leq x \leq 1.0$ )] NPs inhibit the growth of *E. coli* similarly, and they reported MIC and MBC values in the range of 2.5 to >16 mg/mL and 5 to >32mg/ mL, respectively.<sup>10</sup> Another study<sup>29</sup> reported that metal-substituted cobalt ferrite NPs at 5000 ppm inhibits the growth of both gram-negative (*E. coli*) and gram-positive (*S. aureus*) bacterial strains.

## Evaluation of the Anticandidal Activity of NSFs by Colony-Forming Unit (CFU)

The anticandidal activity of  $[\text{Ni}_{0.4}\text{Cu}_{0.2}\text{Zn}_{0.4}](\text{Fe}_{2-x}\text{Dy}_x)\text{O}_4$  ( $x=0, 0.01, 0.02, 0.03$  and  $0.04$ ) NSFs was investigated using the standard colony count method by calculating the percentage survival rate of *C. albicans* cells after treatment with 2 mg/mL of  $x=0, 0.01, 0.02, 0.03$  and  $0.04$  NSFs. It was found that the viable cell count of treated *C. albicans* was significantly less than that of untreated control cells (Figure 6). All five ratios exhibit a pronounced effect on the survival of *C. albicans*, and the survival rate was 23.3, 25, 30.9, 17.7 and 76.5% for ratios  $x=0, 0.01, 0.02, 0.03$  and  $0.04$  NSFs, respectively (Figure 7). It has been found that in comparison to other samples, the ration  $x= 0.03$  displays higher activity, whilst  $x=0.04$  indicates the least activity. Our results are in good agreement with the

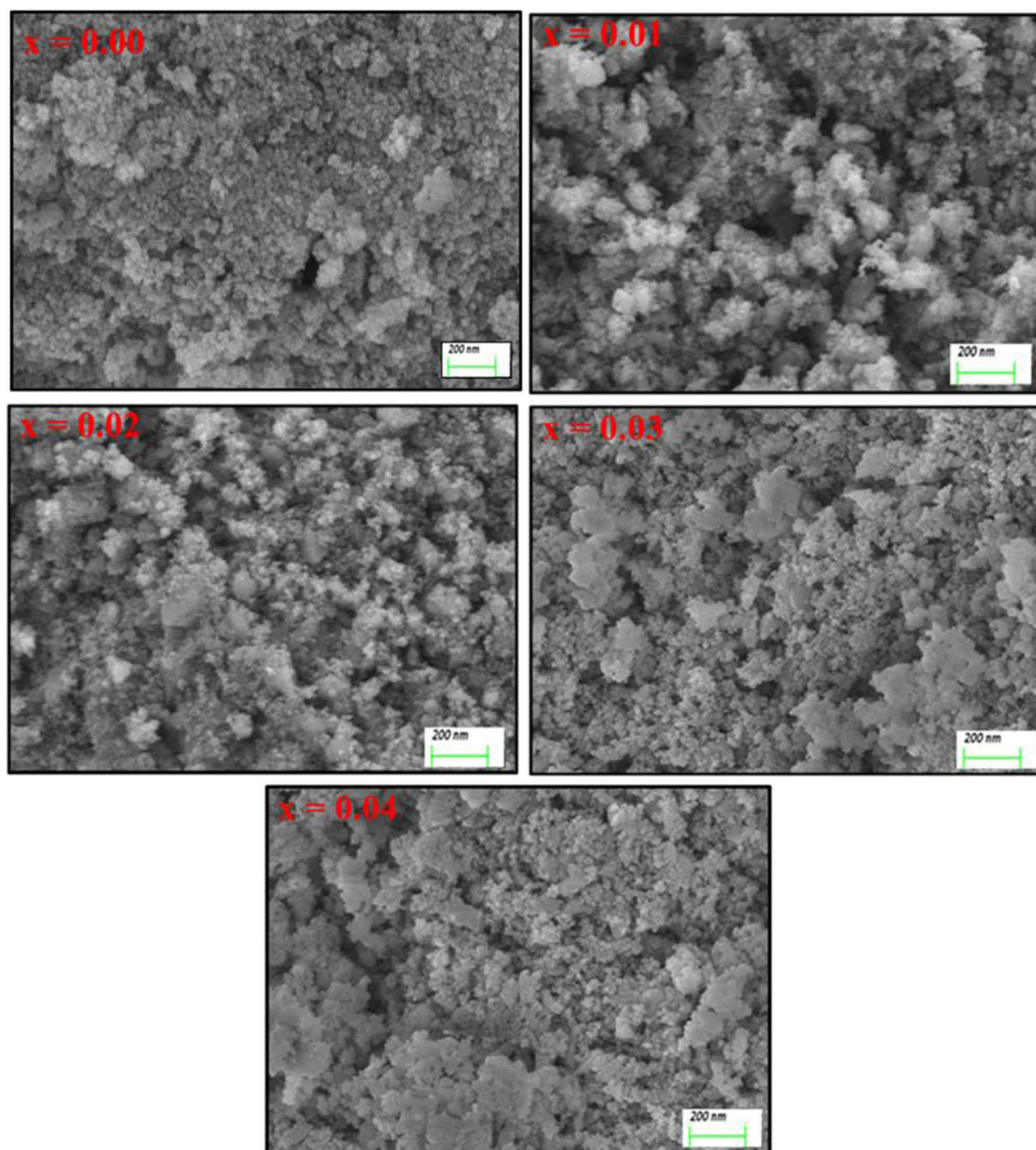


**Figure 2** SEM micrograph of  $[\text{Ni}_{0.4}\text{Cu}_{0.2}\text{Zn}_{0.4}](\text{Fe}_{2-x}\text{Dy}_x)\text{O}_4$  ( $x \leq 0.4$ ) NSFs.

study,<sup>11</sup> where they reported that neodymium (Nd)-substituted cobalt ferrites NPs inhibit the growth of *C. albicans* in a similar pattern. This is the first report of Dy-substituted nickel-copper-zinc nano spinel ferrites with broad-spectrum antimicrobial activity against gram-positive

methicillin-resistant *S. aureus* and the yeast *C. albicans*. Our study found that, as the dopant content, ie, Dy increases from 0.0 to 0.03, the anticandidal activity of NSFs was also increased, which is in agreement with the previous study.<sup>11</sup>

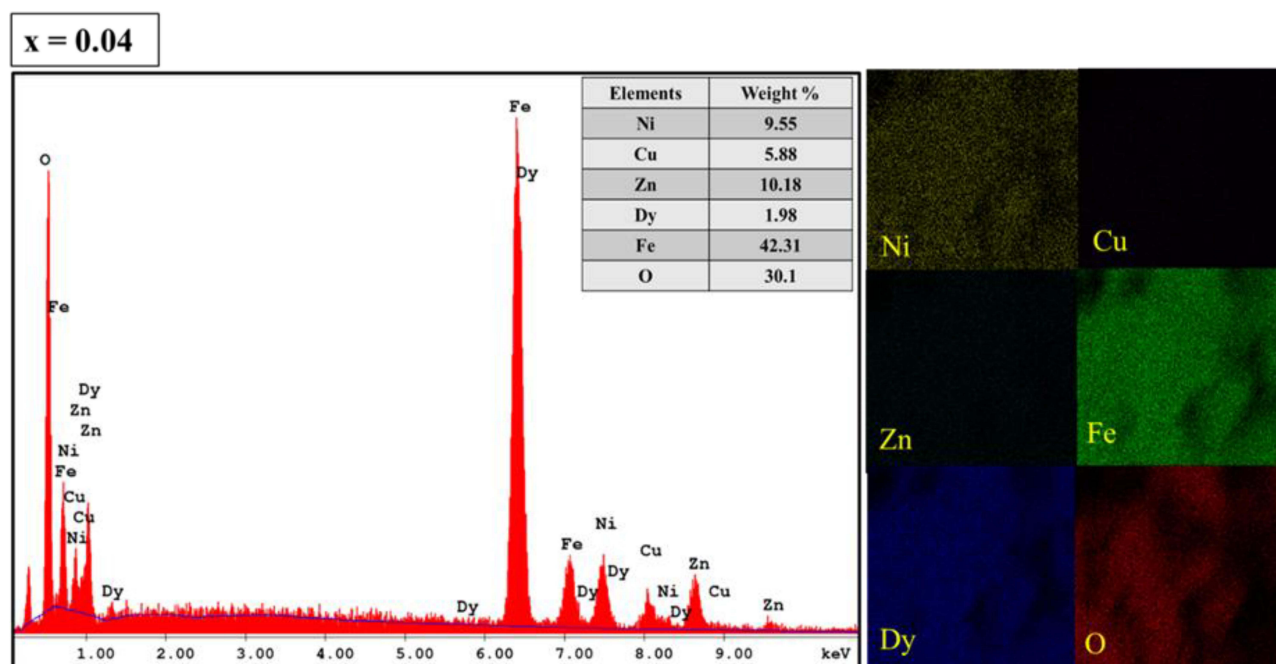


**Figure 3** EDX of SEM micrograph of  $[\text{Ni}_{0.4}\text{Cu}_{0.2}\text{Zn}_{0.4}](\text{Fe}_{2-x}\text{Dy}_x)\text{O}_4$  ( $x=0.4$ ) NSFs.

## Effect of Ni-Cu-Zn NSFs on MRSA and *C. albicans* Biofilms

In the present study, the effects of Ni-Cu-Zn NSFs on the biofilm-forming abilities of MRSA and *C. albicans* were assessed by a quantitative 96-well microtiter polystyrene plate assay. It was found that 1 mg/mL of Ni-Cu-Zn NSFs ie,  $x=0.0$ ,  $x=0.01$ ,  $x=0.02$ ,  $x=0.03$  and  $x=0.04$  inhibit biofilm formation by 27.6%, 26.2%, 58.5%, 33.3% and 25% for MRSA and 47.5%, 43.5%, 48.6%, 58.3% and 26.6% for *C. albicans*, respectively (Figure 8).

Further, to visualize the effect of Ni-Cu-Zn NSFs on biofilm of MRSA and *C. albicans* formed on glass surface was examined by SEM (Figures 9 and 10). It was found that the untreated (control) glass coverslips support the adherence, colonization and aggregation of large numbers of MRSA cells (Figure 9A). However, MRSA biofilm treated with Ni-Cu-Zn NSFs display significantly reduced the adherence and colonization of cells and scattered cells with loss of cell wall and membrane was also seen (Figure 9B), indicating the brutal damage of biofilm architecture and EPS matrix.

The biofilm of untreated (control) *C. albicans* grown on glass coverslips showed a characteristic intense network of hyphae and highly aggregated cells (Figure 10A). After treatment with Ni-Cu-Zn NSFs, reduced biofilm formation

was seen which was primarily comprised of scattered individual cells (Figure 10B). It was also observed that the treated biofilm of *C. albicans* had almost no true hyphae and the number of cells was significantly reduced (Figure 10B).

## Topological Changes Caused by NSFs on MRSA and Candida Cells: SEM Analysis

The effects of  $[\text{Ni}_{0.4}\text{Cu}_{0.2}\text{Zn}_{0.4}](\text{Fe}_{2-x}\text{Dy}_x)\text{O}_4$  ( $x \leq 0.04$ ) NSFs on the topological and morphological structure of MRSA and *C. albicans* were also studied by SEM. The untreated control MRSA cells were intact, regular, normal, and spherical, with a smooth cell surface (Figure 11A). However, MRSA cells treated with  $x=0.02$  NSFs showed that the cells were severely damaged, and the number of cells was also significantly reduced. The cell surface was irregular, rough, distorted, and non-intact with the deformed cell membrane and cell wall, indicating loss of integrity of the membrane that ultimately causes cell death (Figure 11B). Similarly, in *C. albicans*, the untreated cells were normal, intact and oval with a smooth cell wall and membrane (Figure 12A). However, the *C. albicans* cells treated with  $x=0.02$  NSFs showed significant cell damage, and the cell surface was

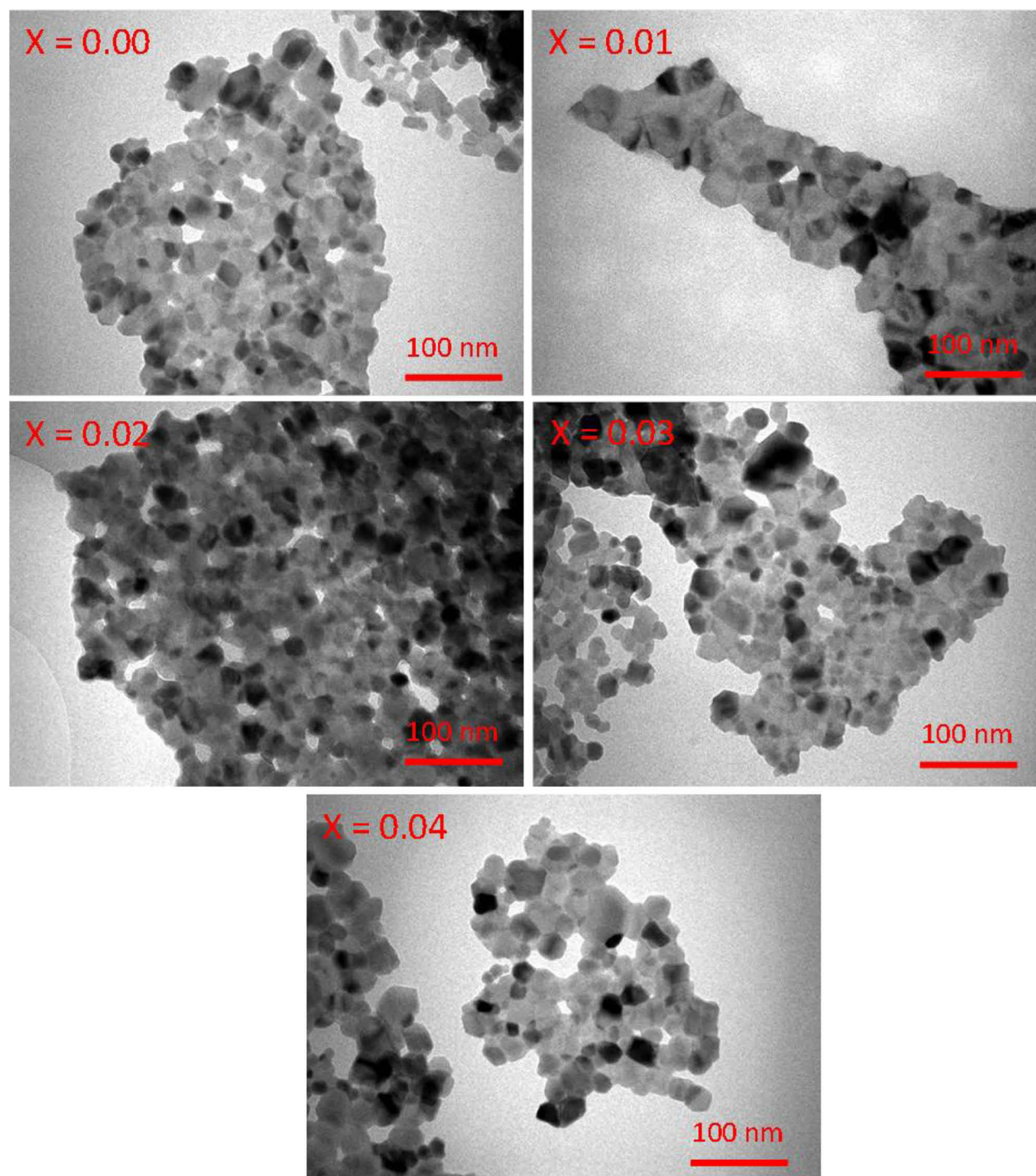


**Figure 4** TEM micrograph of  $[\text{Ni}_{0.4}\text{Cu}_{0.2}\text{Zn}_{0.4}](\text{Fe}_{2-x}\text{Dy}_x)\text{O}_4$  ( $x \leq 0.4$ ) NSFs.

rough and irregular. Most importantly, the number of *C. albicans* cells dramatically decreased, and the severely damaged cells were no longer intact, which

may ultimately cause cell death (Figure 12B). Our results are in good agreement with the study of Ansari et al<sup>10</sup> and Rehman et al.<sup>11</sup>



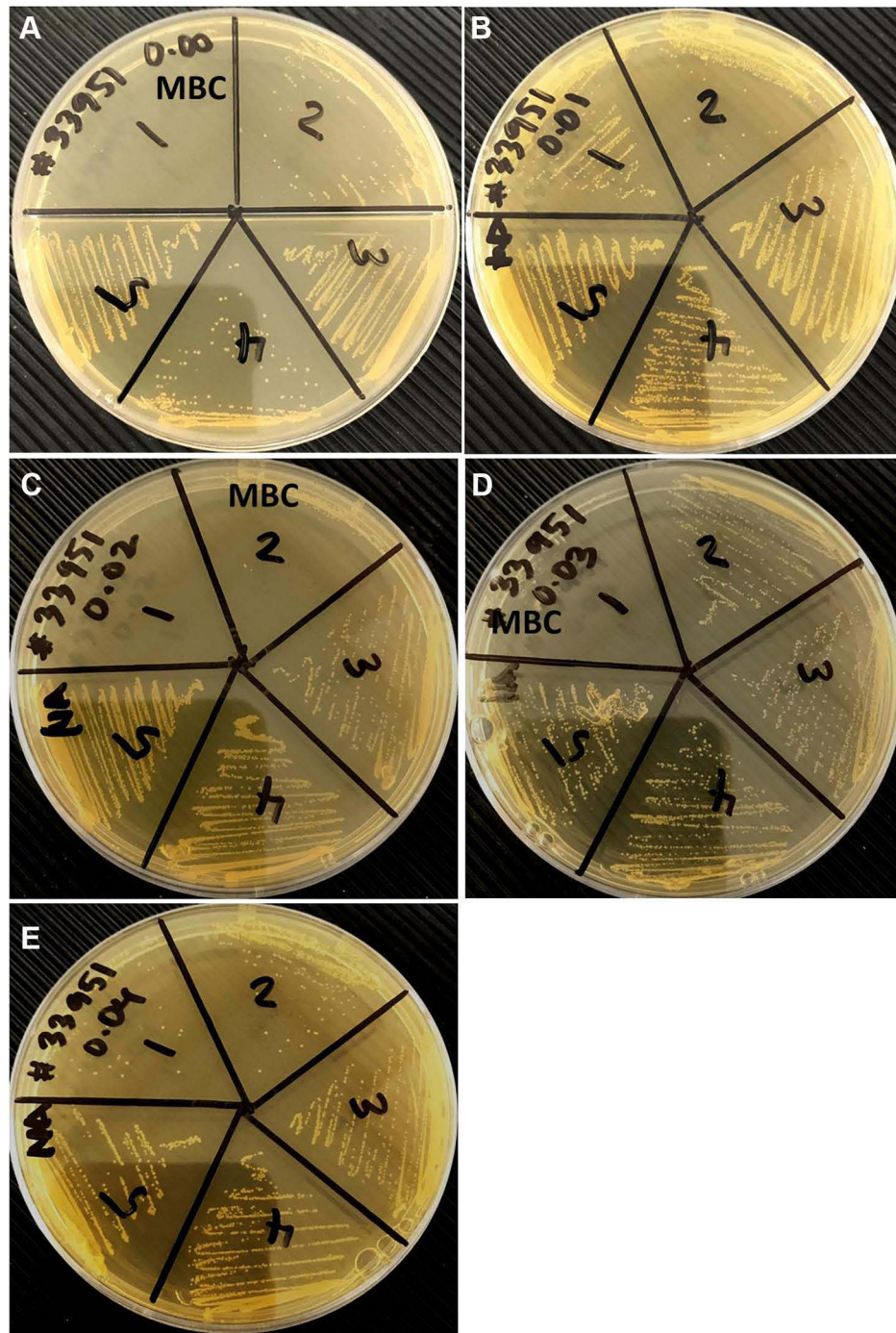


**Figure 5** Nutrient agar plates showing MBC (mg/mL) values of  $[\text{Ni}_{0.4}\text{Cu}_{0.2}\text{Zn}_{0.4}](\text{Fe}_{2-x}\text{Dy}_x)\text{O}_4$  ( $x \leq 0.4$ ) NSF against MRSA. Panels (A–E) represent samples with  $x=0.0$ ,  $x=0.01$ ,  $x=0.02$ ,  $x=0.03$ , and  $x=0.04$ , respectively. The concentrations of NSF are represented by the numbers 1, 2, 3, 4, and 5, which are 16, 8, 4, 2, and 1 mg/mL, respectively.

### Ultrastructural Alteration Caused by NSF on MRSA and Candida Cells: TEM Analysis

Furthermore, the effects of  $[\text{Ni}_{0.4}\text{Cu}_{0.2}\text{Zn}_{0.4}](\text{Fe}_{2-x}\text{Dy}_x)\text{O}_4$  ( $x \leq 0.04$ ) NSF on the ultrastructure of MRSA and

*C. albicans* cells were investigated by TEM analysis. The untreated MRSA cell showed standard cell features, eg, regular, smooth and intact and well-preserved cell wall and membrane (Figure 13A). However, substantial ultrastructural alteration such as brutal damage of cell wall and

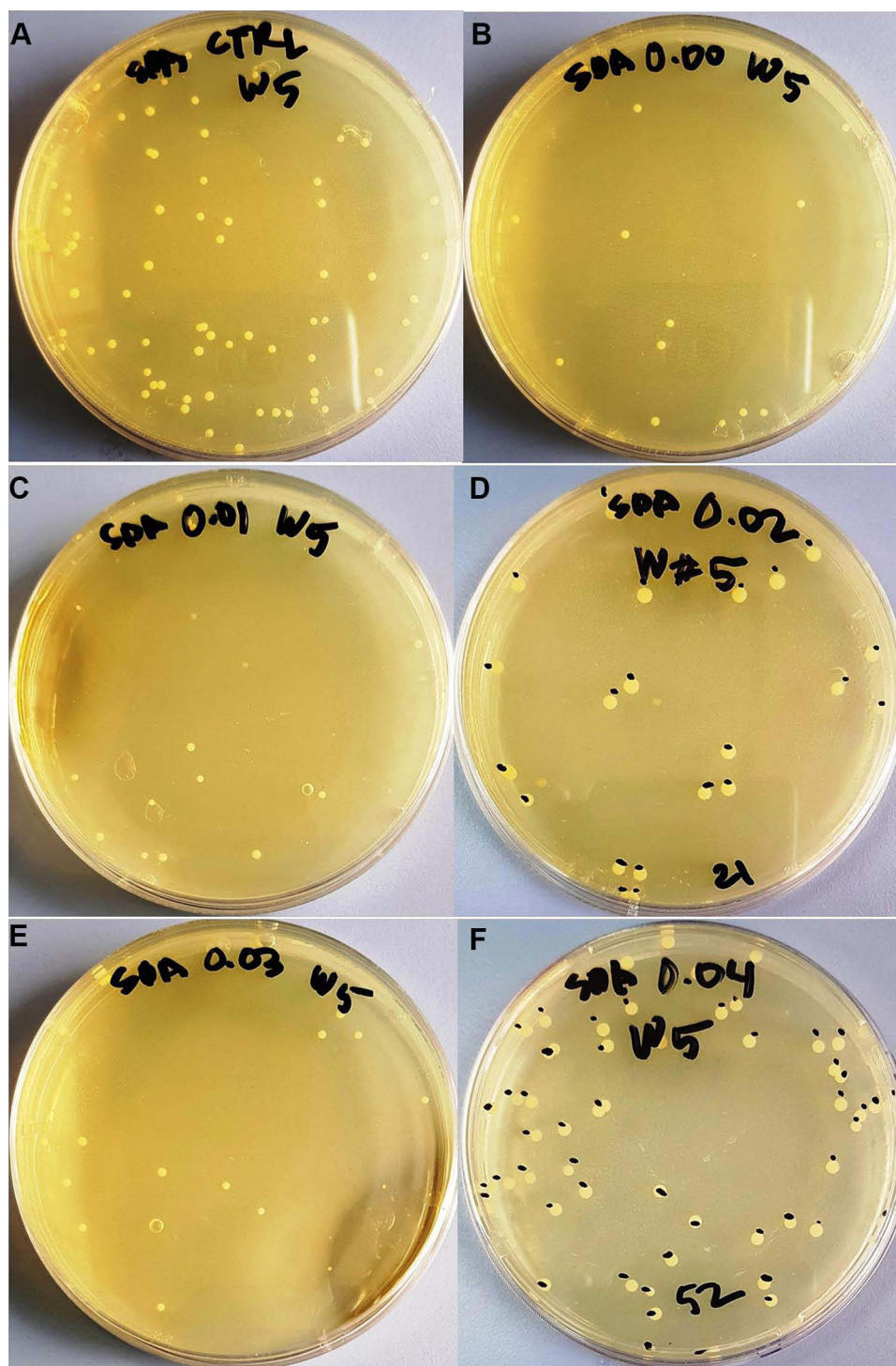


**Figure 6** SDA culture plates showing the CFU of *C. albicans* treated with 1 mg/mL of  $[\text{Ni}_{0.4}\text{Cu}_{0.2}\text{Zn}_{0.4}](\text{Fe}_{2-x}\text{Dy}_x)\text{O}_4$  ( $x \leq 0.04$ ) NSFs. (A) Untreated cells, (B)  $x=0.0$ , (C)  $x=0.01$ , (D)  $x=0.02$ , (E)  $x=0.03$  and (F)  $x=0.04$ .

membrane was seen in MRSA cells treated with NSFs. It was also observed that the treated cells were abnormal, irregular and severely broken down into fragments. Apart from cell wall damage, apparent separation and

disintegration of cell wall and membrane from the cell was also seen (Figure 13). TEM analysis also shows the adsorption, internalization and penetration of NSFs inside the cells causes rupturing of the cell membrane.

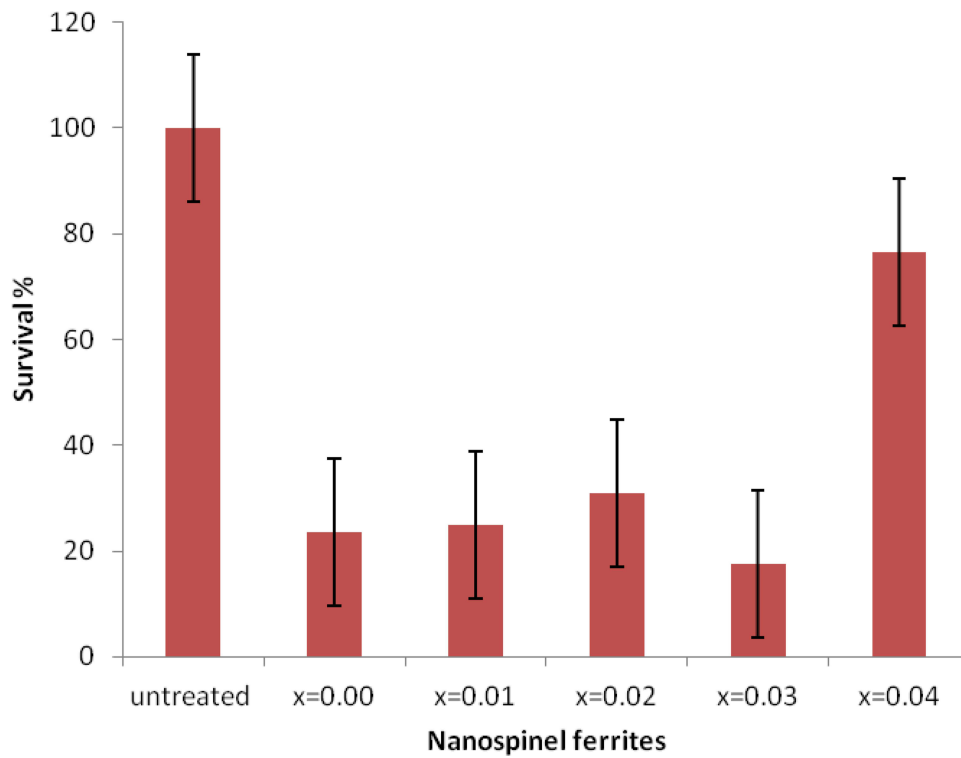


**Figure 7** Survival rate (%) of *C. albicans* treated with 1 mg/mL of  $[\text{Ni}_{0.4}\text{Cu}_{0.2}\text{Zn}_{0.4}](\text{Fe}_{2-x}\text{Dy}_x)\text{O}_4$  ( $x \leq 0.04$ ) NSFs.

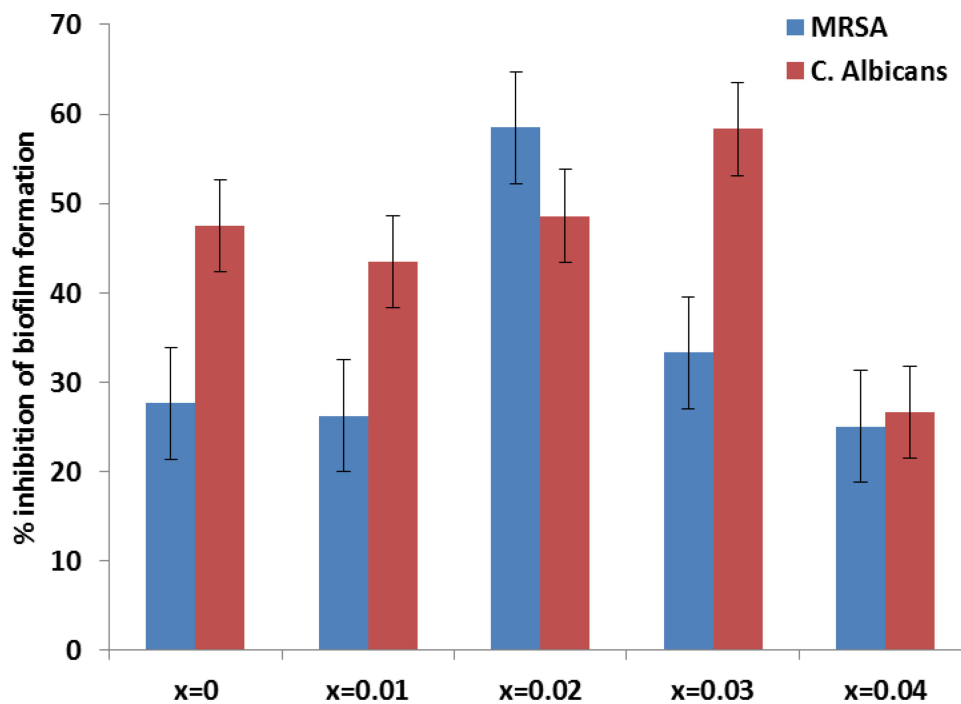


**Figure 8** Effect of  $[\text{Ni}_{0.4}\text{Cu}_{0.2}\text{Zn}_{0.4}](\text{Fe}_{2-x}\text{Dy}_x)\text{O}_4$  ( $x \leq 0.04$ ) NSFs on biofilm forming abilities of MRSA and *C. albicans* biofilm at 1 mg/mL.

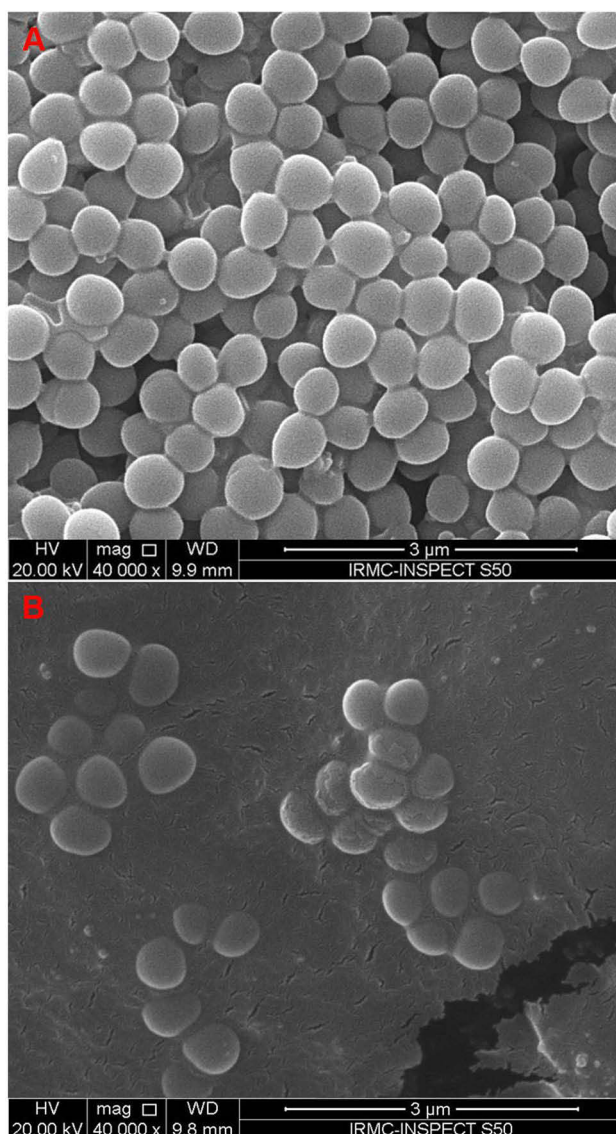


**Figure 9** Microscopic analysis of biofilm inhibition. SEM micrographs of biofilm formed by MRSA grown in absence (A) and presence of  $[\text{Ni}_{0.4}\text{Cu}_{0.2}\text{Zn}_{0.4}](\text{Fe}_{2-x}\text{Dy}_x)\text{O}_4$  ( $x = 0.02$ ) NSF (B).

Furthermore, large clear hollows were also seen in the cytoplasm that causes leakage of cytoplasmic content from a cell that may lead to the destabilization of the cell wall and membrane integrity that finally led to the cell death (Figure 13B and C). The TEM images of untreated *C. albicans* cells shows that the yeast cells were typically oval with a regular, smooth and intact cell wall and membrane (Figure 14A and B). However, *C. albicans* cell treated with NSFs were in an abnormal

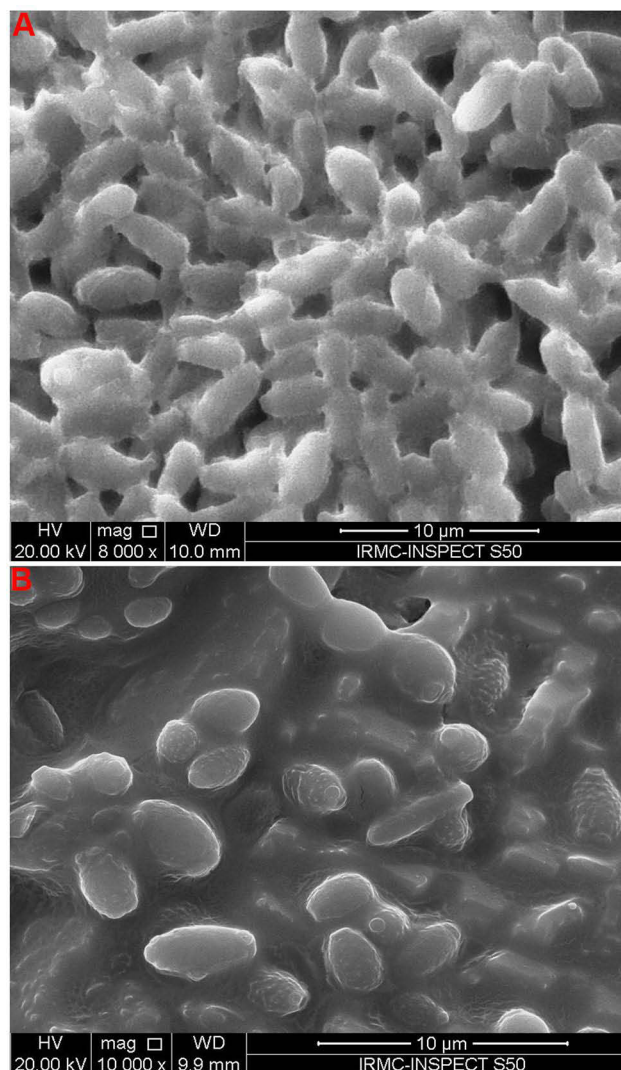


**Figure 10** Microscopic analysis of biofilm inhibition. SEM micrographs of biofilm formed by *C. albicans* grown in absence (A) and presence of  $[\text{Ni}_{0.4}\text{Cu}_{0.2}\text{Zn}_{0.4}](\text{Fe}_{2-x}\text{Dy}_x)\text{O}_4$  ( $x = 0.03$ ) NSF (B).

condition with irregular fragments appearing on the cell surfaces (Figure 14C and D), and the cell was severely damaged, showing deformation, distortion and separation of cell wall and membrane, indicating a significant loss of membrane integrity that may lead to cell death (Figure 14C and D).

The exact antimicrobial activity and mode of action of spinel ferrite nanoparticles are still not understood. However, there are some studies where it has been reported that the antimicrobial activity of spinel NPs was due to the adsorption and penetration of spinel ferrite NPs by bacteria and yeast cells that leads to disorganization of cell membrane and wall,

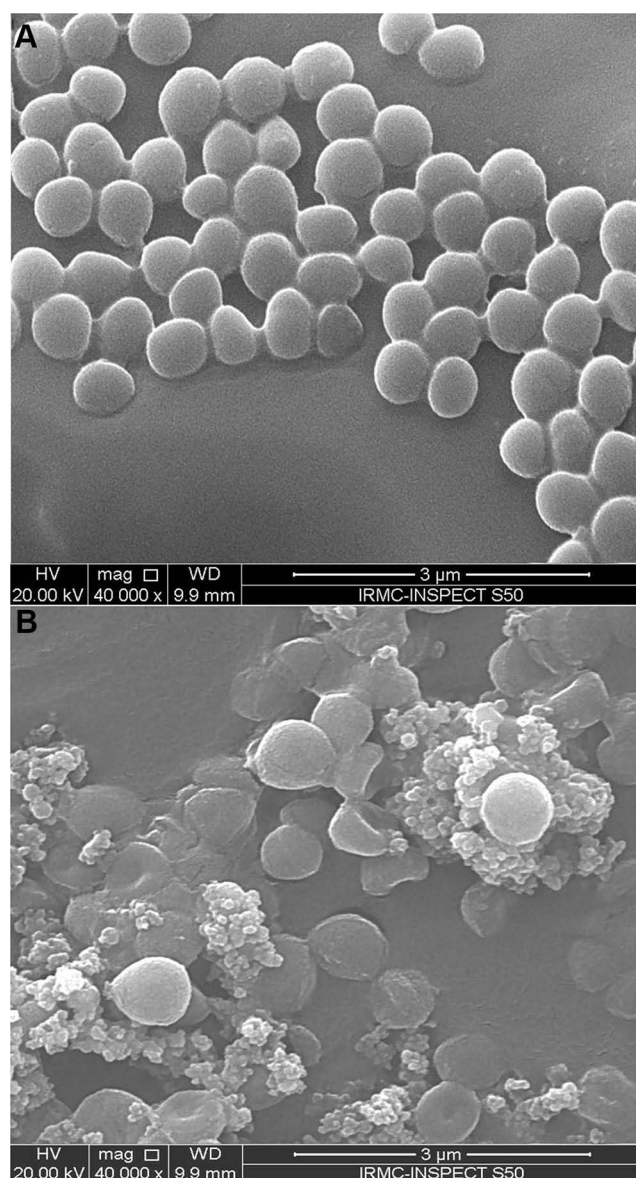


**Figure 11** Interaction between  $[\text{Ni}_{0.4}\text{Cu}_{0.2}\text{Zn}_{0.4}](\text{Fe}_{2-x}\text{Dy}_x)\text{O}_4$  ( $x = 0.02$ ) NSF and MRSA cells. **(A)** Represent SEM images of MRSA cells in the absence of NSF. Whereas, **(B)** demonstrate cellular damage in MRSA cells in the presence of  $[\text{Ni}_{0.4}\text{Cu}_{0.2}\text{Zn}_{0.4}](\text{Fe}_{2-x}\text{Dy}_x)\text{O}_4$  ( $x = 0.02$ ) NSF.

followed by the leakage of various cytoplasmic content might be a possible mode of action.<sup>10,11,30</sup> In the present study, TEM images clearly show that NSF get attached to bacteria and yeast's cell surface and subsequently damage the cytoplasmic membrane, possibly due to interaction between nanoparticles and cell membrane.<sup>30,31</sup> Further, the attachment of NPs also causes the depolarization of the cell wall, which alters the negative charge of the cell surface to become more permeable.<sup>11,32,33</sup> The generation of reactive oxygen species (ROS) by nanoparticles might be another possible

antimicrobial mechanism mode. Another report by Simon-Deckers et al<sup>34</sup> reported that ROS generation by NPS might prevent the DNA replication that may lead to cell death. In the present study, we assumed that NSF might generate ROS that electrostatically interact with cell walls and cause damage to bacteria and yeast cells. Sanpo also reported that the generation of ROS from spinel metal substituted cobalt ferrite nanoparticles has more potential to enter the cell wall and inhibit *E. coli* and *S. aureus*.<sup>28</sup> In another study, it was proposed that ROS generated from the NPs surface interacts with the cell membrane that may damage the membrane due to increased cell permeability and leakage of the intracellular materials.<sup>35,36</sup> From SEM and TEM analysis, we suggested that disruption, disorganization and disintegration of the cell membrane by NPs might be the primary cause of cell death. Furthermore, the intracellular leakage of cytoplasmic content due to the loss of membrane integrity may cause the detachment of cell membrane that eventually leads to the complete lysis of MRSA and yeast cells as supported by TEM micrographs (Figures 13 and 14).

## Cytotoxic Activity

Based on our antibacterial and antifungal activity of NSF, we investigated the cytotoxic effects of NSF ( $x=0.02$  and  $x=0.03$ ) on HCT-116 cells using the MTT cell viability assay. The cell viability assay revealed a significant decrease in cell viability following NSF ( $x=0.02$  and  $x=0.03$ ) treatment. It was observed that NSF ( $x=0.02$  and  $x=0.03$ ) inhibited cancer cell growth and proliferation in a dose-dependent manner (Figure 15). The cell viability was  $92.23 \pm 0.64\%$ ,  $24.58 \pm 1.88\%$ ,  $21.77 \pm 2.69\%$  and  $16.83 \pm 1.59\%$  when HCT-116 cells were treated with NSF ( $x=0.02$ ) at concentrations of 2, 5, 15 and 45  $\mu\text{g}/\text{mL}$ , respectively; whereas when treated with NSF ( $x=0.03$ ) at similar concentrations, the cell viability was  $96 \pm 2\%$ ,  $80.65 \pm 3.58\%$ ,  $40.62 \pm 1.1\%$  and  $32.11 \pm 1.53\%$ , respectively (Figure 15). Furthermore, the  $\text{IC}_{50}$  values for NSF ( $x=0.02$ ) and ( $x=0.03$ ) were examined as 5 and 15  $\mu\text{g}/\text{mL}$ , respectively. The current study's findings are consistent with a previously published report.<sup>26,27</sup>

## Observation of Disintegration of Cancer DNA

The treatment of HCT-116 cells with NSF ( $x=0.02$  and  $x=0.03$ ) caused a significant decrease in the number of colon cancer cells as compared to control cells

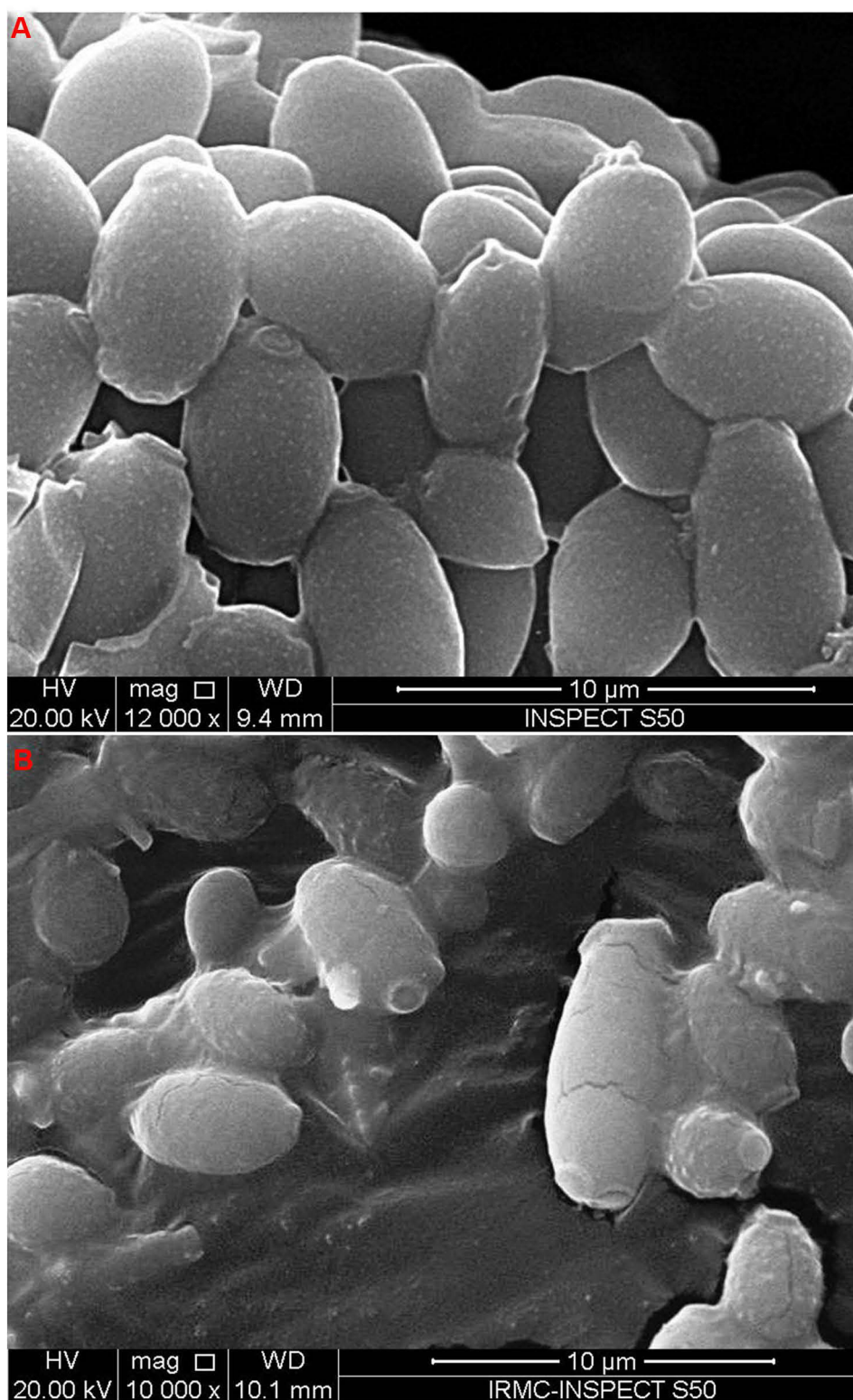


**Figure 12** Interaction between  $[\text{Ni}_{0.4}\text{Cu}_{0.2}\text{Zn}_{0.4}](\text{Fe}_{2-x}\text{Dy}_x)\text{O}_4$  ( $x = 0.02$ ) NSFs and *C. albicans* cells. **(A)** Represent SEM images of *C. albicans* cells in the absence of NSFs. Whereas, **(B)** demonstrate cellular damage in *C. albicans* cells in presence of  $[\text{Ni}_{0.4}\text{Cu}_{0.2}\text{Zn}_{0.4}](\text{Fe}_{2-x}\text{Dy}_x)\text{O}_4$  ( $x = 0.03$ ) NSFs.

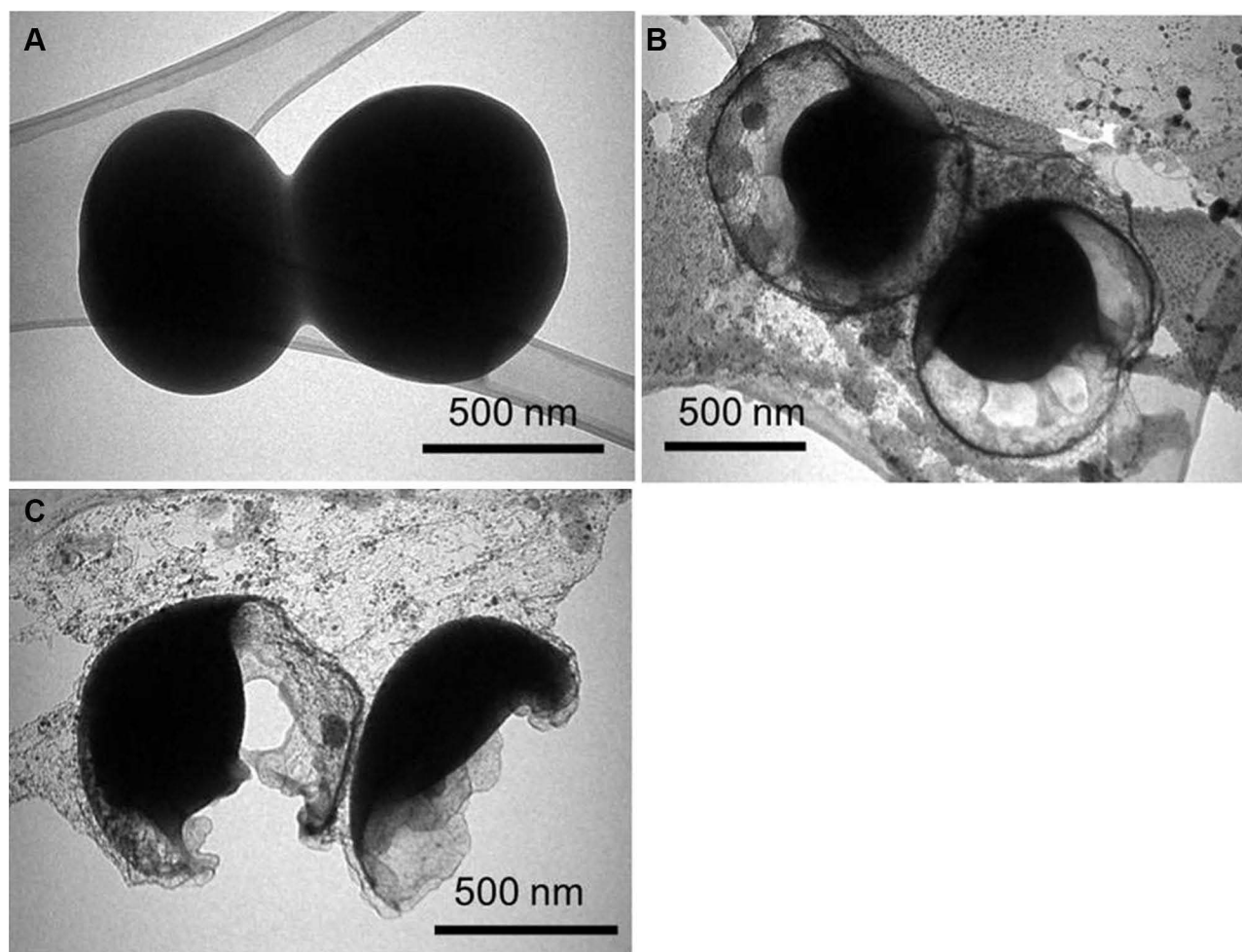


**Figure 13** TEM images of the control and treated MRSA cells. The control cells were normal, and their cell membrane was normal, regular and intact (A). The cells treated with  $[\text{Ni}_{0.4}\text{Cu}_{0.2}\text{Zn}_{0.4}](\text{Fe}_{2-x}\text{Dy}_x)\text{O}_4$  ( $x = 0.02$ ) NSF were abnormal, irregular and they lost their cell integrity as the cell membrane and cell wall was severely damaged that shows internalization of NSFs (B and C).

(Figure 16B and C). The reduction in cancer cells is due to cell death, which is probably due to programmed cell death or apoptosis. In NSF-treated cells, DAPI staining revealed apoptotic morphological alterations, including nuclear condensation and cell structure destruction. In contrast, the control cells did not show any inhibitory action and cells remained intact, and retained their normal anatomical and morphological structure (Figure 16A). The findings of the current study are in line with those of the previous investigation.<sup>26,28,37</sup>

## Conclusion

In summary,  $[\text{Ni}_{0.4}\text{Cu}_{0.2}\text{Zn}_{0.4}](\text{Fe}_{2-x}\text{Dy}_x)\text{O}_4$  ( $x \leq 0.04$ ) nano spinel ferrites with increased antibacterial, antifungal, antibiofilm and anticancer activity against Gram-positive bacteria MRSA, yeast *C. albicans* and colon cancer cells has been investigated.

Both bacteria and yeast, as well as cancer cells, are inhibited by the NSF. In addition to their profound antimicrobial studies, the NSF demonstrated a strong ability to prevent MRSA and *C. albicans* biofilm formation and disruption of biofilm matrix. The TEM analysis of bacteria and *Candida* reveals large ultra-structural changes as well as severe damage to cell wall and membrane, indicating a significant loss of membrane integrity, which ultimately results in cell death. The findings indicate that the NSF holds significant therapeutic promise in the treatment of bacterial and fungal biofilm infections, particularly those caused by medical devices. The quality and properties of NSF can be improved and enhanced by coating or functionalizing their surface with non-toxic chemicals, which could present a promising opportunity for future generations to solve medical and environmental problems. Furthermore, it has been suggested that incorporating NSF into novel materials or devices

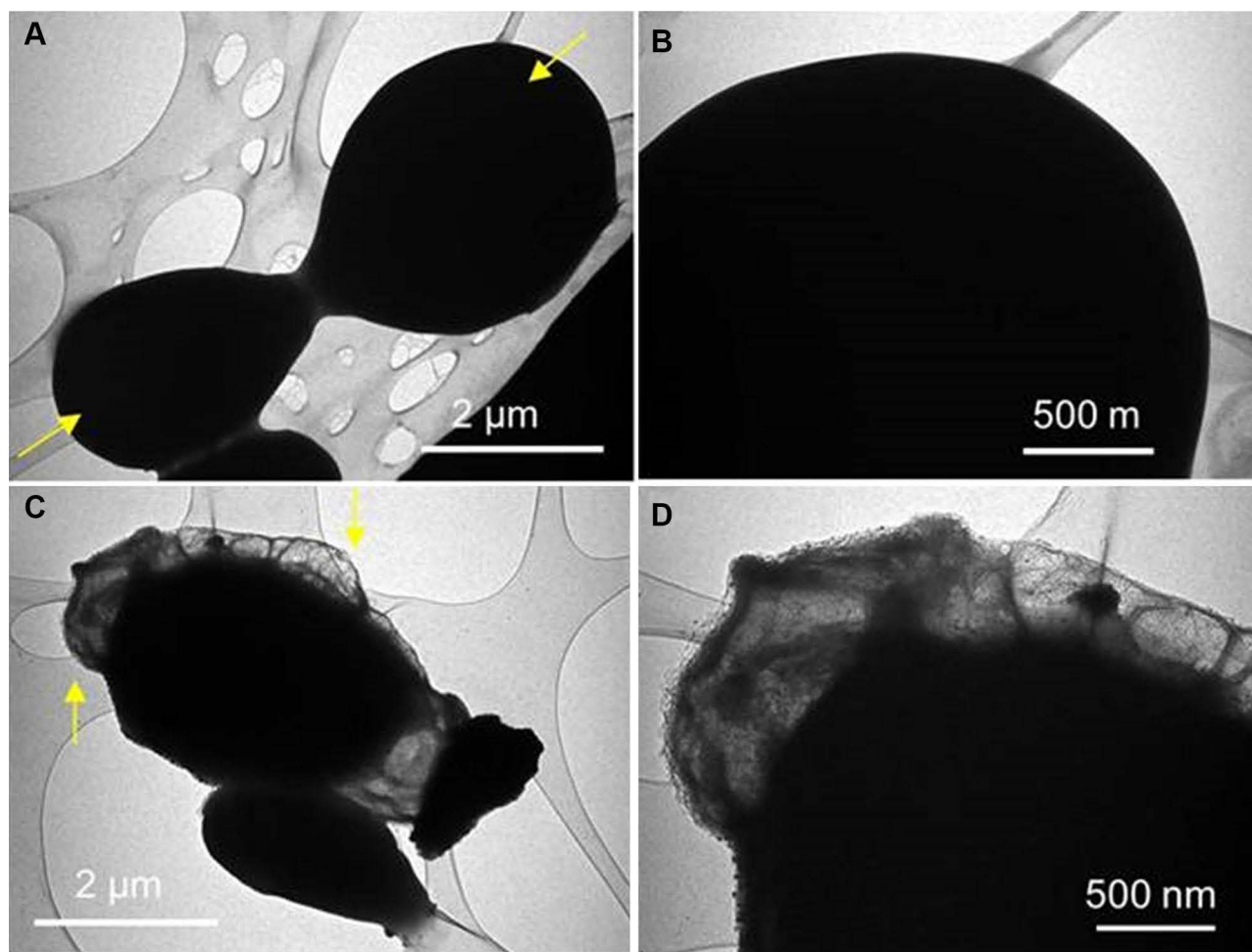


**Figure 14** TEM images of the control and treated *C. albicans* cells. The control cells were normal, and their membrane was intact (**A** and **B**). The cells treated with  $[\text{Ni}_{0.4}\text{Cu}_{0.2}\text{Zn}_{0.4}](\text{Fe}_{2-x}\text{Dy}_x)\text{O}_4$  ( $x = 0.03$ ) NSFs were abnormal, and they lost their cell integrity as the cell membrane was severely damaged that shows internalization of NSFs (**C** and **D**). The yellow arrows show the cells or the parts of the cells that were zoomed in the next images.

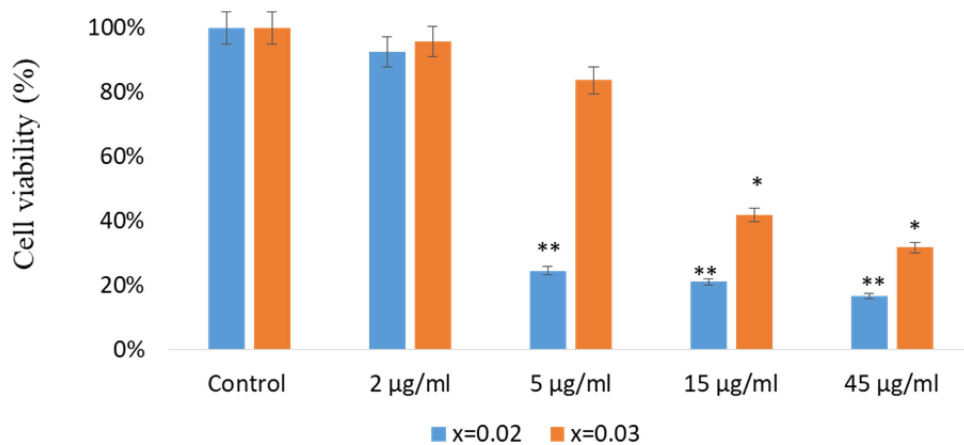


**Figure 15** Dose-dependent cytotoxic activity of NSFs ( $x=0.02$  and  $x=0.03$ ) toward HCT-116 cells estimated by MTT assay. Asterisks indicate significant differences between the viability of cells.

**Notes:** (\* $p < 0.05$ ; \*\* $p < 0.01$ ).



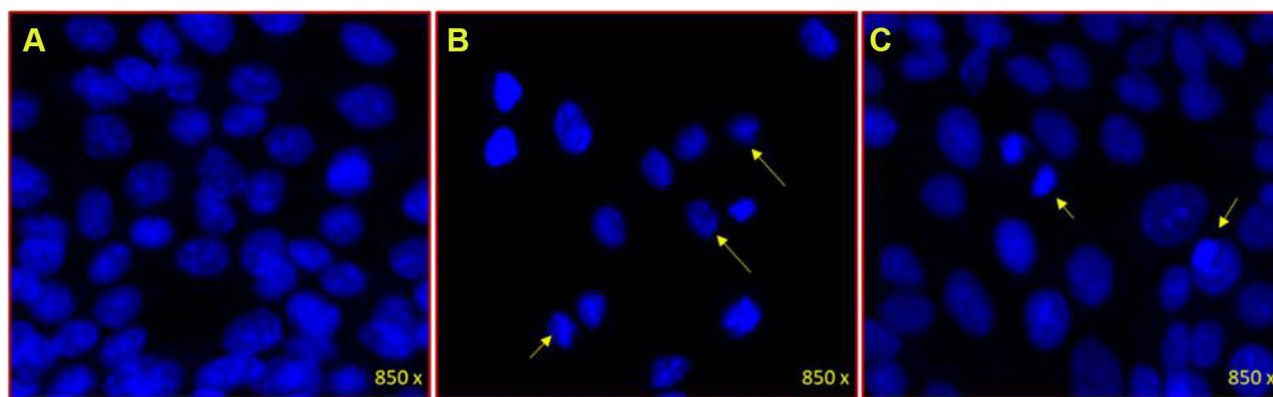


**Figure 16** Morphology of DAPI stained cancer cells after 48 h of treatment. (A) represents control, whereas (B and C) represent HCT-116 cells treated with 35  $\mu\text{g/mL}$  of NSF ( $x=0.02$ ), and ( $x=0.03$ ), respectively. Arrows indicate cell disintegration, and cell chromatin condensation and fragmentation.

could provide additional promising features for disease detection, identification, and treatment. Furthermore, while the application of NSF in several biomedical fields appears to be important, the risk and in vivo toxicity of NSF should be carefully evaluated and explored in detail prior to commercialization or widespread use. Therefore, the necessary measurements should be conducted in order to reduce the unforeseen outcomes in a variety of biomedical applications.

## Acknowledgments

The authors extend their appreciation to the Deputyship for Research & Innovation, “Ministry of Education” in Saudi Arabia for funding this research work through the project number IFKSURG-2020-142. The authors would like thanks to Institute for Research and Medical Consultation (IRMC), Imam Abdulrahman Bin Faisal University, Dammam, Saudi Arabia, providing technical, administrative support and facilities to carry out the research work.

## Disclosure

The authors report no conflicts of interest in this work.

## References

- Jin J, Zhu S, Song Y, et al. Precisely controllable core-shell Ag@carbon dots nanoparticles: application to in situ super-sensitive monitoring of catalytic reactions. *ACS Appl Mater Interfaces*. 2016;8(41):27956–27965. doi:10.1021/acsami.6b07807
- Wang J. Nanomaterial-based electrochemical biosensors. *Analyst*. 2005;130(4):421–426. doi:10.1039/b414248a
- Kefeni KK, Msagati TAM, Nkambule TTI, Mamba BB. Spinel ferrite nanoparticles and nanocomposites for biomedical applications and their toxicity. *Mater Sci Eng C*. 2020;40(107):110314.
- Nakamura T. Snoek’s limit in high-frequency permeability of polycrystalline Ni–Zn, Mg–Zn, and Ni–Zn–Cu spinel ferrites. *J Appl Phys*. 2000;88(1):348–353. doi:10.1063/1.373666
- Yadav RS, Kuřitka I, Vilcakova J, et al. Structural, magnetic, dielectric, and electrical properties of NiFe<sub>2</sub>O<sub>4</sub> spinel ferrite nanoparticles prepared by honey-mediated sol-gel combustion. *J Physics Chem Solids*. 2017;107:150–161. doi:10.1016/j.jpcs.2017.04.004
- Hsieh YK, Jiang PS, Yang BS, Sun TY, Peng HH, Wang CF. Using laser ablation/inductively coupled plasma mass spectrometry to bioimage multiple elements in mouse tumors after hyperthermia. *Anal Bioanal Chem*. 2011;401(3):909–915. doi:10.1007/s00216-011-5144-7
- Reddy MP, Balakrishnaiah G, Madhuri W, et al. Structural, magnetic and electrical properties of NiCuZn ferrites prepared by microwave sintering method suitable for MLCI applications. *J Physics Chem Solids*. 2010;71(9):1373–1380. doi:10.1016/j.jpcs.2010.06.007
- Mazumdar SC, Alam F, Tanni UH, Kali K, Das BC, Khan MN. Effect of Ti<sup>4+</sup> doping on structural, electrical and magnetic properties of Ni<sub>0.4</sub>Cu<sub>0.2</sub>Zn<sub>0.4</sub>Fe<sub>2-x</sub>Ti<sub>x</sub>O<sub>4</sub> ferrites. *Mater Sci Appl*. 2019;10(12):733. doi:10.4236/msa.2019.1012053
- Samavati A, Ismail AF. Antibacterial properties of copper-substituted cobalt ferrite nanoparticles synthesized by co-precipitation method. *Particuology*. 2017;30:158–163. doi:10.1016/j.partic.2016.06.003
- Ansari MA, Baykal A, Asiri S, Rehman S. Synthesis and characterization of antibacterial activity of spinel chromium-substituted copper ferrite nanoparticles for biomedical application. *J Inorg Organomet Polym Mater*. 2018;28(6):2316–2327. doi:10.1007/s10904-018-0889-5
- Rehman S, Ansari MA, Alzohairy MA, et al. Antibacterial and antifungal activity of novel synthesized neodymium-substituted cobalt ferrite nanoparticles for biomedical application. *Processes*. 2019;7(10):714. doi:10.3390/pr7100714
- Esmaili M, Dezhampanah H, Hadavi M. Surface modification of super paramagnetic iron oxide nanoparticles via milk casein for potential use in biomedical areas. *J Biomol Struct Dyn*. 2021;39(3):977–987. doi:10.1080/07391102.2020.1722751
- Shahabadi N, Hadidi S, Shiri F. New water-soluble Fe<sub>3</sub>O<sub>4</sub>@SiO<sub>2</sub> magnetic nanoparticles functionalized with levetiracetam drug for adsorption of essential biomolecules by case studies of DNA and HSA. *J Biomol Struct Dyn*. 2020;38(1):283–294. doi:10.1080/07391102.2019.1569557
- Amiri M, Salavati-Niasari M, Akbari A. Magnetic nanocarriers: evolution of spinel ferrites for medical applications. *Adv Colloid Interface Sci*. 2019;265:29–44. doi:10.1016/j.cis.2019.01.003
- Naskar A, Kim KS. Nanomaterials as delivery vehicles and components of new strategies to combat bacterial infections: advantages and limitations. *Microorganisms*. 2019;7(9):356. doi:10.3390/microorganisms7090356
- Naskar A, Lee S, Lee Y, Kim S, Kim KS. A new nano-platform of erythromycin combined with Ag nano-particle ZnO nano-structure against methicillin-resistant Staphylococcus aureus. *Pharmaceutics*. 2020;12(9):841. doi:10.3390/pharmaceutics12090841

17. Naskar A, Lee S, Kim KS. Au–ZnO conjugated black phosphorus as a near-infrared light-triggering and recurrence-suppressing nanoantibiotic platform against *Staphylococcus aureus*. *Pharmaceutics*. 2021;13(1):52. doi:10.3390/pharmaceutics13010052
18. Cho H, Naskar A, Lee S, Kim S, Kim KS. A new surface charge neutralizing nano-adjuvant to potentiate polymyxins in killing Mcr-1 mediated drug-resistant *Escherichia coli*. *Pharmaceutics*. 2021;13(2):250. doi:10.3390/pharmaceutics13020250
19. Goyal A, Bansal S, Singhal S. Facile reduction of nitrophenols: comparative catalytic efficiency of MFe<sub>2</sub>O<sub>4</sub> (M= Ni, Cu, Zn) nano ferrites. *Int J Hydrogen Energy*. 2014;39(10):4895–4908. doi:10.1016/j.ijhydene.2014.01.050
20. Ahmed MA, Mansour SF, Afifi M. Structural and electrical properties of nanometric Ni–Cu ferrites synthesized by citrate precursor method. *J Magn Magn Mater*. 2012;324(1):4–10. doi:10.1016/j.jmmm.2011.07.010
21. Su H, Zhang H, Tang X, Jia L, Wen Q. Sintering characteristics and magnetic properties of NiCuZn ferrites for MLCI applications. *Mater Sci Eng B*. 2006;129(1–3):172–175. doi:10.1016/j.mseb.2006.01.008
22. Ansari MA, Asiri SM, Alzohairy MA, Alomary MN, Almatroudi A, Khan FA. Biofabricated fatty acids-capped silver nanoparticles as potential antibacterial, antifungal, antibiofilm and anticancer agents. *Pharmaceutics*. 2021;14(2):139. doi:10.3390/ph14020139
23. Ali SG, Ansari MA, Jamal QM, et al. Butea monosperma seed extract mediated biosynthesis of ZnO NPs and their antibacterial, antibiofilm and anti-quorum sensing potentialities. *Arab J Chem*. 2021;14(4):103044. doi:10.1016/j.arabjc.2021.103044
24. Elsharif AM, Youssef TE, Al-Jameel SS, et al. Synthesis of an activatable tetra-substituted nickel phthalocyanines-4 (3H)-quinazolinone conjugate and its antibacterial activity. *Adv Pharmacol Sci*. 2019;17. doi:10.1155/2019/5964687
25. Ansari MA, Khan HM, Khan AA, Cameotra SS, Saquib Q, Musarrat J. Interaction of Al<sub>2</sub>O<sub>3</sub> nanoparticles with *Escherichia coli* and their cell envelope biomolecules. *J Appl Microbiol*. 2014;116(4):772–783. doi:10.1111/jam.12423
26. Aljameel SS, Almessiere MA, Khan FA, et al. Synthesis, characterization, anti-cancer analysis of Sr<sub>0.5</sub>Ba<sub>0.5</sub>DyxSmxFe<sub>8–2x</sub>O<sub>19</sub> (0.00 ≤ x ≤ 1.0) microsphere nanocomposites. *Nanomaterials*. 2021;11(3):700. doi:10.3390/nano11030700
27. Alahmari F, Rehman S, Almessiere M, Khan FA, Slimani Y, Baykal A. Synthesis of Ni<sub>0.5</sub>Co<sub>0.5</sub>CdxFe<sub>1.78</sub>Nd<sub>0.02</sub>O<sub>4</sub> (x ≤ 0.25) nanofibers by using electrospinning technique induce anti-cancer and anti-bacterial activities. *J Biomol Struct Dyn*. 2021;39(9):3186–3193.
28. Sanpo N, Wen C, Berndt CC, Wang J. *Antibacterial Properties of Spinel Ferrite Nanoparticles. Microbial Pathogens and Strategies for Combating Them: Science, Technology and Education*. Spain: Formatex Research Centre; 2013:239–250.
29. Ashour AH, El-Batal AI, Maksoud MA, et al. Antimicrobial activity of metal-substituted cobalt ferrite nanoparticles synthesized by sol-gel technique. *Particuology*. 2018;40(1):141–151. doi:10.1016/j.partic.2017.12.001
30. Barathiraja C, Manikandan A, Uduman Mohideen AM, Jayasree S, Antony SA. Magnetically recyclable spinel Mn<sub>x</sub>Ni<sub>1-x</sub>Fe<sub>2</sub>O<sub>4</sub> (x= 0.0–0.5) nano-photocatalysts: structural, morphological and optomagnetic properties. *J Superconduct Novel Magnet*. 2016;29:477–486. doi:10.1007/s10948-015-3312-2
31. Jiang W, Mashayekhi H, Xing B. Bacterial toxicity comparison between nano- and micro-scale oxide particles. *Environ Pollut*. 2009;157:1619–1625. doi:10.1016/j.envpol.2008.12.025
32. Rauf MA, Owais M, Rajpoot R, Ahmad F, Khan N, Zubair S. Biomimetically synthesized ZnO nanoparticles attain potent antibacterial activity against less susceptible *S. aureus* skin infection in experimental animals. *RSC Adv*. 2017;7(58):36361–36373. doi:10.1039/C7RA05040B
33. Stoimenov PK, Klinger RL, Marchin GL, Klabunde KJ. Metal oxide nanoparticles as bactericidal agents. *Langmuir*. 2002;18(17):6679–6686. doi:10.1021/la0202374
34. Simon-Deckers A, Loo S, Mayne-L'hermite M, et al. Size-, composition- and shape-dependent toxicological impact of metal oxide nanoparticles and carbon nanotubes toward bacteria. *Environ Sci Technol*. 2009;43(21):8423–8429. doi:10.1021/es9016975
35. Leung YH, Xu X, Ma AP, et al. Toxicity of ZnO and TiO<sub>2</sub> to *Escherichia coli* cells. *Sci Rep*. 2016;6(1):1–13. doi:10.1038/srep35243
36. Liu S, Zeng TH, Hofmann M, et al. Antibacterial activity of graphite, graphite oxide, graphene oxide, and reduced graphene oxide: membrane and oxidative stress. *ACS Nano*. 2011;5(9):6971–6980. doi:10.1021/nn202451x
37. Rehman S, Almessiere MA, Khan FA, et al. Synthesis and biological characterization of Mn<sub>0.5</sub>Zn<sub>0.5</sub>O. 5EuxDyxFe<sub>1.8–2x</sub>O<sub>4</sub> nanoparticles by sonochemical approach. *Mater Sci Eng C*. 2020;109:110534. doi:10.1016/j.msec.2019.110534

## International Journal of Nanomedicine

### Publish your work in this journal

The International Journal of Nanomedicine is an international, peer-reviewed journal focusing on the application of nanotechnology in diagnostics, therapeutics, and drug delivery systems throughout the biomedical field. This journal is indexed on PubMed Central, MedLine, CAS, SciSearch®, Current Contents®/Clinical Medicine,

Journal Citation Reports/Science Edition, EMBase, Scopus and the Elsevier Bibliographic databases. The manuscript management system is completely online and includes a very quick and fair peer-review system, which is all easy to use. Visit <http://www.dovepress.com/testimonials.php> to read real quotes from published authors.

Submit your manuscript here: <https://www.dovepress.com/international-journal-of-nanomedicine-journal>